Mathematical Modelling in Civil Engineering
Vol. 18-No. 2: 35-55-2023
10.2478/mmce-2023-0009

ARTIFICIAL NEURAL NETWORK APPROACH TO PREDICT CARBONATION DEPTH IN METAKAOLIN, BRICK POWDER AND CALCINED SEDIMENTS-MODIFIED MORTARS

SOUHEYLA BENAMAR - PhD Student, Smart Structures Laboratory (SSL), Dept. of Civil Engineering & Public Works, University of Aïn-Témouchent, P.B.284, Aïn-Témouchent - 46000 -Algeria, e-mail: souheyla.benamar@univ-temouchent.edu.dz

ZINE EL ABIDINE KAMECHE - Lecturer, Smart Structures Laboratory (SSL), Dept. of Civil Engineering & Public Works, University of Aïn-Témouchent, P.B.284, Aïn-Témouchent - 46000 - Algeria, e-mail: zkameche@univ-temouchent.edu.dz

SIDI MOHAMED AISSA MAMOUNE - Lecturer, Smart Structures Laboratory (SSL), Dept. of Civil Engineering & Public Works, University of Aïn-Témouchent, P.B.284, Aïn-Témouchent - 46000 - Algeria, e-mail: mamoune@univ-temouchent.edu.dz

HOCINE SIAD - Lecturer, Dept. of Civil Engineering, Toronto Metropolitan University. 350, Victoria St., Toronto, ON M5B 2K3, Canada, e-mail: hsiad@ryerson.ca

YOUCEF HOUMADI - Lecturer, Smart Structures Laboratory (SSL), Aïn-Témouchent University, Department of Civil Engineering, Tlemcen University, P. Box : 119, Tlemcen - 13000 - Algeria, e-mail: houmadiyoucef@yahoo.fr

Abstract: This research uses Artificial Neural Network (ANN) as a soft computing technique to predict the carbonation depth and service life of cementitious materials with low clinker content. For this purpose, different mortars were prepared with 0, 10, 15, 20, 25 and 30% replacement levels of cement by metakaolin (MK), brick powder (BP) and calcined sediments (CS). The experimental results of the carbonation depth were obtained under natural and accelerated carbonation conditions for exposure periods of 12 months and 28 days respectively. ANN was utilized taking into account the main influential factors on mortars carbonation, including mix proportions and environmental conditions. For the ANN model, seven datasets were considered as inputs, covering mineral admixture content, cement content, curing time, CO_2 concentration, relative humidity, temperature and CO_2 exposure time, in addition to one output parameter which is the carbonation depth. The results show that the resistance to carbonation of the mortars decreases with the increase of cement substitution by MK, BP or CS. The network model gives good performance values in the validation and testing set with a lower mean square error (MSE) and a higher determination coefficient (*R*). The predicted carbonation depths are in good agreement with the experimental measurements of carbonation depths, confirming the efficiency of the developed ANN model to be applied to correctly estimate the carbonation depth of cementitious materials with low clinker content.

Keywords: mortar; carbonation depth prediction; artificial neural network; metakaolin; brick powder; calcined sediments.

1. Introduction

The rapid development of the construction industry has induced a lot of environmental problems over the last decades [1], especially for the cement industry that is responsible alone for 6–7% of global CO_2 emissions [2, 3] and 5% of anthropogenic greenhouse gases (GHGs) emissions [4, 5].

In addition, the increasing trend of the generated waste from construction and demolition activities has also raised concerns about their detrimental impact on the solid waste streams around the world. For these reasons, many researchers have been recently directed into reducing CO_2 emissions and global warming potential from the building sector. These efforts have resulted in important ecological techniques that explore the partial replacement of cement with supplementary cementitious materials (SCMs) to reduce the demand for natural resources and the dependency to clinker in cementitious binders. However, more efficient green alternatives to PC were also investigated through the recycling of waste materials, such as construction and demolition waste (CDW) often abandoned in nature, [6-9]. Similarly, some bio-source materials like dam sediments were successfully used as mineral admixtures in the manufacturing process of cementitious materials.

Metakaolin (MK) resulting from kaolin calcination at a temperature ranging between 600°C and 900°C was widely used to prepare high-performance concretes [10]. Indeed, it is known as a highly efficient pozzolanic material [11], which can improve the mechanical properties and durability of cementitious composites [11-17].

Brick waste, as one of the mainland-filled CDWs and dredged sediments from the cleaning operations of sedimented dams are other clayey materials which were proven with an effective pozzolanic activity, though the heat treatment was necessary to attain a sufficient dehydroxylated and completely amorphous material, close to metakaolin [18-25]. Both materials contain large amounts of amorphous silica and alumina, which can help forming additional hydration products through their reaction with calcium hydroxide [7, 23]. In addition to their filling effect, the pozzolanic activity of brick powder and dredged sediment was shown to improve the mechanical and durability properties of concretes [26-30].

The carbonation phenomenon is identified as one of the foremost causes of premature degradation in cementitious structures [31-33], which can lead to the corrosion of reinforced concrete. It is a natural physicochemical process caused by the reaction between carbon dioxide, penetrating into the concrete pores from the atmosphere, and the hydrated cement compounds ($Ca(OH)_2$ and CSH). This is followed by the precipitation of various calcium carbonate phases ($CaCO_3$) [34, 35]. This dissolution–reprécipitation process may gradually reduce the alkalinity and pH of the pore solution of cementitious materials from a value higher than 12.5 to lower than 9 [36].

The effect of using metakaolin, brick powder and dredged sediments on the carbonation resistance of cementitious materials has been studied by several researchers; nevertheless, conflicting results can be found in the literature regarding the incorporation of each mineral admixture. Some authors have concluded that the substitution of cement with MK significantly decreases the rate and depth of carbonation [37-39]. Likewise, brick powder has been found by Schackow et al. [18] to reduce the carbonation rate due to its pozzolanic reaction development over time, leading to the densification of the cement matrix and resulting in a total decrease in porosity [40-42]. In addition, Safer [43] reported a positive effect of substituting cement with calcinated mud, since the depth of natural carbonation of concrete mixed with 10 to 30% of calcinated mud was significantly lower than that of the control concrete.

On the other hand, several studies [23, 44, 45] have reported that the carbonation depth increases with the increase in the substitution of cement by metakaolin, brick powder or dredged sediments. This was explained by the consumption of portlandite by the pozzolanic reaction, which promoted the early carbonation of calcium silicate hydrate (CSH) in the case of cementitious materials with mineral admixtures [44]. It is generally agreed that carbonation does not occur in the same way in all mixes. Thus, the discrepancies in carbonation results are mainly due to the fact that the carbonation phenomenon depends on several factors, including the mix proportions of cementitious materials (mineral admixture and cement content, curing conditions, binder chemical composition) and the exposure conditions (temperature, relative humidity, CO_2 concentration) [46, 47]. Consequently, considering these factors in any experimental and/or theoretical study is fundamental to embracing all the parameters related to the carbonation phenomenon.

Several studies, such as Van Balen and Van Gemert [48] and Papadakis [49], agree on the fact that the carbonation depth can be expressed by a mathematical relation. However, the complexity of the numerical calculation associated with the assessment of carbonation depth dependency on each factor, requires the use of special computational methods for determining the general relationship between abundant and complex information. In this matter, Artificial Neural Network (ANN) [50] was adopted by many specialists to predict the carbonation of concretes since it models almost any complex relationship and nonlinear problems between the inputs and outputs [51], according to the Science Direct database [52], in the last decade, 396 papers were published relating to concrete carbonation modelling, which contains 13% of studies that employed ANN model. Most of the existing studies have investigated the carbonation properties of cementitious materials and proposed some models to predict their carbonation depths [47, 53, 54]. For instance, Kwon and Song [55] estimated the CO_2 diffusion coefficients with three input neurons, through a neural network algorithm. They found maximum differences of 6.3% between the estimated and experimental data. Seung and Wang [56] used the results of slag concrete hydration as input parameters with different curing conditions and slag contents to develop the carbonation reaction model. Londhe et al. [57] studied carbonation data from various literatures and proposed an ANN model with the ability to predict the carbonation coefficient as a function of a set of conditioning factors. Furthermore, Taffese et al. [31] have applied the machine learning method for carbonation prediction based on different input parameters, which are stated to control the carbonation process. This study revealed that the developed model has predicted the carbonation depth with a high accuracy. The researches of Possan et al. [58] and Luo et al. [59] suggested that ANN can be an effective tool to predict the carbonation depth in concrete, since it can capture the complex relationships among the various parameters to predict the output (depth of carbonation).

However, when it comes to modelling the carbonation of cementitious materials which contain mineral admixtures at low clinker content, the available studies were mostly completed on fly-ash (FA) materials [52, 60]. Kellouche et al. [61] proposed an ANN model to predicate the carbonation of fly-ash concrete taking into account the most influential parameters, including mixture proportions and exposure conditions. The model was helpful in providing the necessary scientific guidance for the durability design of FA-concretes. Jiang et al. [62] predicted the carbonation of high-volume fly-ash concrete by considering the effect of water/binder ratio and cement content on carbonation rate. More recently, Felix et al. [52] applied ANN for predicting the carbonation of FA-concrete. They concluded that ANN with two hidden layers can generate models with R^2 greater than 0.8. Importantly, all these studies agree that the neural networks is a reliable method which help saving energy, time and cost by taking data samples rather than entire data sets to attain the targeted solutions [63].

Although, various models were used to predict the carbonation depth of low clinker concretes, very limited information can be found about the carbonation modelling of cementitious materials containing metakaolin (MK), brick powder (BP) or calcined sediments (CS). Whereas, these admixtures have been used in important construction projects in some countries [64], there is no available literature on comparing the effect of MK, BP and CS on the carbonation of cementitious materials.

This highlights an important knowledge gap, indicating the need for further research to fully understand and ensure the safer application of these SCMs (MK, BP and CS in the construction sector).

This study aims to bridge an important research gap by exploring the utilization of artificial neural network model to predict the effect of different contents of MK, BP and CS on the carbonation depth of low clinker mortar, considering most of the influential parameters on carbonation at two diverse carbonation conditions (natural and accelerated carbonation). The research work was conducted in two steps. First, an experimental program was designed to provide better understanding of the influence of metakaolin, brick waste and dredged sediments as SCMs on the carbonation process of cement mortars. As a second step, the obtained database of carbonation depths of MK, BP and CS-modified mortars was used to ANN analyzes for carbonation depth prediction. Training, validation and testing of the ANN model stages were performed using 192 experimental measurements of accelerated and natural carbonation depths of mortars tested at different ages and for different carbonation exposure times. The model considered seven input data-sets, including mix proportions and environmental conditions, and one output which is the carbonation depth. The obtained results from the network were compared with the experimental results and the performance parameters were determined.

2. Experimental and modelling methods

2.1. Materials

In the present study, Portland cement CEM I 42.5 R complying with the European standard NF EN 197-1 [65] and industrial metakaolin (MK), brick powder (BP) and calcined sediments (CS) were used. The MK and CS are obtained by thermal activation at 850 °C for 3 hours and 750 °C for 3 hours, respectively; it induces the transformation of the crystalline kaolinite into the amorphous metakaolinite phase. While BP was prepared in the laboratory by grinding waste brick elements using a ball mill, then sieving the resulting powder to obtain particles with a diameter < 80 µm. The chemical and physical characteristics of major materials used to produce the mortar mixes are provided in Table 1.

Table 1

Chemical and physical characteristics of cement, MK, BP and CS

Properties		Cement	MK	BP	CS
Chemical composition (%)	CaO	63.41	0.09	14.88	22.30
	SiO_2	20.42	53.90	61.91	49.40
	Al_2O_3	3.96	39.41	14.80	18.61
	Fe_2O_3	5.69	2.50	3.23	8.12
	K_2O	0.31	3.10	2.15	2.74
	MgO	2.43	0.40	2.43	2.58
	Na_2O	0.22	0.09	0.19	0.34
	TiO_2	-	0.23	-	0.13
	SO_3	2.32	-	-	-
	I.R	0.23	-	-	-
	Loss on ignition	0.92	6.50	1.40	5.20
Physical properties	Specific gravity (g/cm^3)	3.12	2.42	2.65	2.59
	Fineness (cm^2/g)	3220	125900	7140	8452

2.2. Mortar mixtures

Sixteen mortar formulations with constant water-to-binder ratio (w/b) of 0.5 were prepared according to the standard NF EN 196-1 [66]. The mortar mixes had proportions of 1/3 (binder/sand). The mixtures were obtained by mass substitution of 10%, 15%, 20%, 25% and 30% of Portland cement by: (i) metakaolin (MK), (ii) brick powder (BP) and (iii) calcined sediments (CS). A polycarboxylate superplasticizer type CHRYSO Fluid-Premia 180® with a density of 1.05 g/cm^3 was added to all the mixes in order to maintain a constant workability with a very plastic consistency (10s - 20s).

The mortars were cast in prismatic moulds (40 × 40 × 160) mm^3 (3 specimens for every batch). After 24 hours, the specimens were demolded and cured in tap water at 20 ± 2°C, up to the testing day.

2.3. Natural and accelerated carbonation test

Three mortar specimens of each mix were tested for both natural and accelerated carbonation tests. After the initial curing ages of 28 and 90 days, a first series of mortar

specimens were exposed to accelerated carbonation in an environmental test chamber at an ambient temperature of 20 ± 2°C, a relative humidity of 66 ± 2% and a CO_2 concentration of 50%, according to the AFGC–AFREM protocol recommended [67]. Similarly, after the same initial curing ages (28 and 90 days), a second series of the mortar specimens were exposed to a natural environment of around 0.04% CO_2 [68] (natural carbonation).

Table 2 reports the considering parameters used, where M_A, C, C_T, C_{CO2}, RH, T, E_T, and C_D refer to the type and content of mineral admixture (MK, BP and CS), cement content, curing time, CO_2

concentration, relative humidity, temperature, CO_2 exposure time and carbonation depth, respectively. Note that, the contents of mineral admixtures (M_A) and cement (C) were obtained by manual measurements, using a balance (weight) (accuracy ± 0.001g). For the CO_2 concentration (C_{CO2}), relative humidity (RH) and temperature (T), were taken from the climatic control chamber for the accelerated carbonation and by a portable measuring instrument (thermo-hygrometer measuring temperature, humidity and CO_2 concentration) for the natural carbonation.

The carbonation depth (C_D) was determined by the dyeing method as explained below. The carbonated mortar specimens (40 × 40 × 160) mm^3 were divided equally into two parts and the inner sides were sprayed with (1%) phenolphthalein solution. Subsequently, it was necessary to wait 30 min for the transition zone to be clearly visible. The phenolphthalein indicator color turns purple at a pH above 9 (non-carbonated zone). The carbonated zones of specimens are the areas where the mortar color is unchanged. The carbonation depth of mortar specimens used was determined by manual measurements, using a Vernier caliper ruler (accuracy ± 0.01mm). The carbonation depth is defined as the average of four measurements corresponding to the four sides of the cross-sectional area of carbonated mortar specimens (40 × 40) mm^2. The carbonation depth was measured after 7, 14, and 28 days of exposure to accelerated carbonation, and after 90, 180 and 360 days of exposure to natural carbonation. The experimental data gathered from these experiments were with a total of 192 carbonation depths measured (see Table 2).

2.4. Statistical analysis

A primarily data preprocessing of the carbonation depth measurements was determined through a statistical analysis, as shown in Table 3. The values gathered in Table 3 can provide a general idea about the typical information of the measured parameters considered in this study (M_A, C, C_T, C_{CO2}, RH, T, E_T and C_D). It is clearly noticeable from Table 3 that the carbonation depth ranges from 0 to 14.8 mm, which indicates the presence of data that has relevance for significant carbonation depths.

Table 4 shows the data correlation coefficients of the studied parameters, which helps drive the ANN model to the correct information about cause–effect relationships of these parameters (M_A, C, C_T, C_{CO2}, RH, T and E_T) and carbonation depths (C_D). Furthermore, to better estimate the carbonation depth, a regression analysis of carbonation depth versus M_A, C, C_T, C_{CO2}, RH, T, and E_T was carried out, as provided in Table 5. *R* square is calculated for linear and quadratic model. It appears that the quadratic model gives the best regression analysis of the data, and the *R* square estimation is most appropriate between the carbonation depth (C_D) and the CO_2 exposure time (E_T). It is around 57% for the linear model and 62% for the quadratic model, but *R* square for both models are lower than the statistical analysis coefficient ($R^2 < 70\%$) as it is determined in the works of Benjamin and Cornell [69].

The carbonation rate in mortars depends on various factors, including mix proportions (mineral admixture content (M_A), cement content (C), water-to-binder ratio (w/b)) and exposure conditions (curing time (C_T), CO_2 concentration (C_{CO2}), relative humidity (RH), temperature (T), and CO_2 exposure time (E_T)). Therefore, it is suggested to use the most powerful modelling technique [70], which has the capacity to model linear and nonlinear systems without making hypothesis implicitly by performing nonlinear function approximation [71]. In this study, the prediction of carbonation depths of mortars is performed using an artificial neural network (ANN).

Table 2

Database used in ANN modelling

			Input parameters							Output
N°	M_A	M_A (%)	M_A (g)	C (g)	C_T (days)	C_{CO2} (%)	RH (%)	T (°C)	E_T (days)	C_D (mm)
Accelerated Carbonation										
1		0 (Control mortar)	0	450.0	28	50	66	20	7	0
2	MK	10	45	405.0	28	50	66	20	7	0
3	MK	15	67.5	382.5	28	50	66	20	7	1
4	MK	20	90	360	28	50	66	20	7	1
5	MK	25	112.5	337.5	28	50	66	20	7	1.5
6	MK	30	135	315	28	50	66	20	7	1.5
7	BP	10	45	405	28	50	66	20	7	0
8	BP	15	67.5	382.5	28	50	66	20	7	1
9	BP	20	90	360	28	50	66	20	7	1
10	BP	25	112.5	337.5	28	50	66	20	7	1
11	BP	30	135	315	28	50	66	20	7	1.5
12	CS	10	45	405	28	50	66	20	7	1
13	CS	15	67.5	382.5	28	50	66	20	7	1
14	CS	20	90	360	28	50	66	20	7	1
15	CS	25	112.5	337.5	28	50	66	20	7	1
16	CS	30	135	315	28	50	66	20	7	1.2
17		0 (CM)	0	450.0	28	50	66	20	14	1.8
18	MK	10	45	405.0	28	50	66	20	14	2
19	MK	15	67.5	382.5	28	50	66	20	14	2.1
20	MK	20	90	360	28	50	66	20	14	2.8
21	MK	25	112.5	337.5	28	50	66	20	14	2.8
22	MK	30	135	315	28	50	66	20	14	3.0
23	BP	10	45	405	28	50	66	20	14	1.8
24	BP	15	67.5	382.5	28	50	66	20	14	2
25	BP	20	90	360	28	50	66	20	14	2.4
26	BP	25	112.5	337.5	28	50	66	20	14	2.4
27	BP	30	135	315	28	50	66	20	14	2.8
28	CS	10	45	405	28	50	66	20	14	2
29	CS	15	67.5	382.5	28	50	66	20	14	2.2
30	CS	20	90	360	28	50	66	20	14	2.5
31	CS	25	112.5	337.5	28	50	66	20	14	2.5
32	CS	30	135	315	28	50	66	20	14	2.9
33		0 (CM)	0	450.0	28	50	66	20	28	6.1
34	MK	10	45	405.0	28	50	66	20	28	8.2
35	MK	15	67.5	382.5	28	50	66	20	28	8.7
36	MK	20	90	360	28	50	66	20	28	9.5
37	MK	25	112.5	337.5	28	50	66	20	28	10.2
38	MK	30	135	315	28	50	66	20	28	10.5
39	BP	10	45	405	28	50	66	20	28	7.7
40	BP	15	67.5	382.5	28	50	66	20	28	8.5
41	BP	20	90	360	28	50	66	20	28	9.8
42	BP	25	112.5	337.5	28	50	66	20	28	9.8
43	BP	30	135	315	28	50	66	20	28	10.0
44	CS	10	45	405	28	50	66	20	28	7.0
45	CS	15	67.5	382.5	28	50	66	20	28	7.4
46	CS	20	90	360	28	50	66	20	28	8.5
47	CS	25	112.5	337.5	28	50	66	20	28	9.4

48		30	135	315	28	50	66	20	28	10.2
49		0 (CM)	0	450.0	**90**	50	66	20	7	0
50	**MK**	10	45	405.0	**90**	50	66	20	7	0
51		15	67.5	382.5	**90**	50	66	20	7	0
52		20	90	360	**90**	50	66	20	7	0
53		25	112.5	337.5	**90**	50	66	20	7	1
54		30	135	315	**90**	50	66	20	7	1
55	**BP**	10	45	405	**90**	50	66	20	7	0
56		15	67.5	382.5	**90**	50	66	20	7	0
57		20	90	360	**90**	50	66	20	7	1
58		25	112.5	337.5	**90**	50	66	20	7	1
59		30	135	315	**90**	50	66	20	7	1
60	**CS**	10	45	405	**90**	50	66	20	7	0
61		15	67.5	382.5	**90**	50	66	20	7	0
62		20	90	360	**90**	50	66	20	7	0
63		25	112.5	337.5	**90**	50	66	20	7	0
64		30	135	315	**90**	50	66	20	7	1
65		0 (CM)	0	450.0	**90**	50	66	20	14	1.3
66	**MK**	10	45	405.0	**90**	50	66	20	14	1.8
67		15	67.5	382.5	**90**	50	66	20	14	2
68		20	90	360	**90**	50	66	20	14	2.1
69		25	112.5	337.5	**90**	50	66	20	14	2
70		30	135	315	**90**	50	66	20	14	2.1
71	**BP**	10	45	405	**90**	50	66	20	14	1.5
72		15	67.5	382.5	**90**	50	66	20	14	1.8
73		20	90	360	**90**	50	66	20	14	2
74		25	112.5	337.5	**90**	50	66	20	14	2.1
75		30	135	315	**90**	50	66	20	14	2.1
76	**CS**	10	45	405	**90**	50	66	20	14	1.8
77		15	67.5	382.5	**90**	50	66	20	14	1.8
78		20	90	360	**90**	50	66	20	14	2.0
79		25	112.5	337.5	**90**	50	66	20	14	2.1
80		30	135	315	**90**	50	66	20	14	2.3
81		0 (CM)	0	450.0	**90**	50	66	20	28	5.7
82	**MK**	10	45	405.0	**90**	50	66	20	28	7.7
83		15	67.5	382.5	**90**	50	66	20	28	8
84		20	90	360	**90**	50	66	20	28	8.5
85		25	112.5	337.5	**90**	50	66	20	28	9.5
86		30	135	315	**90**	50	66	20	28	9.7
87	**BP**	10	45	405	**90**	50	66	20	28	6.2
88		15	67.5	382.5	**90**	50	66	20	28	7
89		20	90	360	**90**	50	66	20	28	7.5
90		25	112.5	337.5	**90**	50	66	20	28	8
91		30	135	315	**90**	50	66	20	28	9.5
92	**CS**	10	45	405	**90**	50	66	20	28	6.4
93		15	67.5	382.5	**90**	50	66	20	28	6.8
94		20	90	360	**90**	50	66	20	28	7.2
95		25	112.5	337.5	**90**	50	66	20	28	8.5
96		30	135	315	**90**	50	66	20	28	9.0
Natural carbonation										
97		0 (Control mortar)	0	450.0	28	0.04	73	10	90	3.0
89	**MK**	10	45	405.0	28	0.04	73	10	90	2.7
99		15	67.5	382.5	28	0.04	73	10	90	3.8

100		20	90	360	28	0.04	73	10	90	3.8
101		25	112.5	337.5	28	0.04	73	10	90	4.0
102		30	135	315	28	0.04	73	10	90	4.2
103		10	45	405	28	0.04	73	10	90	3.1
104		15	67.5	382.5	28	0.04	73	10	90	4.4
105	**BP**	20	90	360	28	0.04	73	10	90	4.8
106		25	112.5	337.5	28	0.04	73	10	90	5.2
107		30	135	315	28	0.04	73	10	90	5.2
108		10	45	405	28	0.04	73	10	90	2.5
109		15	67.5	382.5	28	0.04	73	10	90	3.2
110	**CS**	20	90	360	28	0.04	73	10	90	3.2
111		25	112.5	337.5	28	0.04	73	10	90	3.7
112		30	135	315	28	0.04	73	10	90	4.8
113		0 (CM)	0	450.0	28	0.04	67	15	180	4.5
114		10	45	405.0	28	0.04	67	15	180	4.7
115		15	67.5	382.5	28	0.04	67	15	180	4.7
116	**MK**	20	90	360	28	0.04	67	15	180	5.5
117		25	112.5	337.5	28	0.04	67	15	180	6.4
118		30	135	315	28	0.04	67	15	180	6.2
119		10	45	405	28	0.04	67	15	180	5.5
120		15	67.5	382.5	28	0.04	67	15	180	5.5
121	**BP**	20	90	360	28	0.04	67	15	180	5.8
122		25	112.5	337.5	28	0.04	67	15	180	6.2
123		30	135	315	28	0.04	67	15	180	6.0
124		10	45	405	28	0.04	67	15	180	5.4
125		15	67.5	382.5	28	0.04	67	15	180	5.7
126	**CS**	20	90	360	28	0.04	67	15	180	6.2
127		25	112.5	337.5	28	0.04	67	15	180	6.2
128		30	135	315	28	0.04	67	15	180	6.8
129		0 (CM)	0	450.0	28	0.04	68	23	360	11.2
130		10	45	405.0	28	0.04	68	23	360	12.8
131		15	67.5	382.5	28	0.04	68	23	360	13.2
132	**MK**	20	90	360	28	0.04	68	23	360	13.7
133		25	112.5	337.5	28	0.04	68	23	360	14.5
134		30	135	315	28	0.04	68	23	360	14.8
135		10	45	405	28	0.04	68	23	360	12.7
136		15	67.5	382.5	28	0.04	68	23	360	13.8
137	**BP**	20	90	360	28	0.04	68	23	360	13.8
138		25	112.5	337.5	28	0.04	68	23	360	14.7
139		30	135	315	28	0.04	68	23	360	14.7
140		10	45	405	28	0.04	68	23	360	12.8
141		15	67.5	382.5	28	0.04	68	23	360	12.8
142		20	90	360	28	0.04	68	23	360	13.4
143	**CS**	25	112.5	337.5	28	0.04	68	23	360	13.8
144		30	135	315	28	0.04	68	23	360	14.0
145		0 (CM)	0	450.0	**90**	0.04	70	14	90	2.8
146		10	45	405.0	**90**	0.04	70	14	90	2.2
147		15	67.5	382.5	**90**	0.04	70	14	90	2.4
148	**MK**	20	90	360	**90**	0.04	70	14	90	3.1
149		25	112.5	337.5	**90**	0.04	70	14	90	3.5
150		30	135	315	**90**	0.04	70	14	90	3.5
151		10	45	405	**90**	0.04	70	14	90	1.8
152		15	67.5	382.5	**90**	0.04	70	14	90	2.5
153	**BP**	20	90	360	**90**	0.04	70	14	90	3.2
154		25	112.5	337.5	**90**	0.04	70	14	90	4.0
155		30	135	315	**90**	0.04	70	14	90	4.2

156		10	45	405	**90**	0.04	70	14	90	1.8
157		15	67.5	382.5	**90**	0.04	70	14	90	1.8
158	**CS**	20	90	360	**90**	0.04	70	14	90	2.0
159		25	112.5	337.5	**90**	0.04	70	14	90	2.5
160		30	135	315	**90**	0.04	70	14	90	3.2
161		0 (CM)	0	450.0	**90**	0.04	59	25	180	3.5
162		10	45	405.0	**90**	0.04	59	25	180	3.7
163		15	67.5	382.5	**90**	0.04	59	25	180	4.2
164	**MK**	20	90	360	**90**	0.04	59	25	180	4.7
165		25	112.5	337.5	**90**	0.04	59	25	180	5
166		30	135	315	**90**	0.04	59	25	180	5.5
167		10	45	405	**90**	0.04	59	25	180	2.5
168		15	67.5	382.5	**90**	0.04	59	25	180	3.2
169	**BP**	20	90	360	**90**	0.04	59	25	180	4.5
170		25	112.5	337.5	**90**	0.04	59	25	180	4.5
171		30	135	315	**90**	0.04	59	25	180	5.2
172		10	45	405	**90**	0.04	59	25	180	2.5
173		15	67.5	382.5	**90**	0.04	59	25	180	3.4
174	**CS**	20	90	360	**90**	0.04	59	25	180	3.8
175		25	112.5	337.5	**90**	0.04	59	25	180	4.5
176		30	135	315	**90**	0.04	59	25	180	4.8
177		0 (CM)	0	450.0	**90**	0.04	75	11	360	10.5
178		10	45	405.0	**90**	0.04	75	11	360	11.0
179		15	67.5	382.5	**90**	0.04	75	11	360	11.5
180	**MK**	20	90	360	**90**	0.04	75	11	360	12.2
181		25	112.5	337.5	**90**	0.04	75	11	360	12.5
182		30	135	315	**90**	0.04	75	11	360	13.7
183		10	45	405	**90**	0.04	75	11	360	10.0
184		15	67.5	382.5	**90**	0.04	75	11	360	10.2
185	**BP**	20	90	360	**90**	0.04	75	11	360	11.0
186		25	112.5	337.5	**90**	0.04	75	11	360	11.8
187		30	135	315	**90**	0.04	75	11	360	13.5
188		10	45	405	**90**	0.04	75	11	360	11.0
189		15	67.5	382.5	**90**	0.04	75	11	360	11.4
190	**CS**	20	90	360	**90**	0.04	75	11	360	12.8
191		25	112.5	337.5	**90**	0.04	75	11	360	12.8
192		30	135	315	**90**	0.04	75	11	360	13.0

Table 3

Data statistical analysis

	Number	Minimum	Maximum	Mean	Standard deviation
C (g)	192	315.00	450.00	365.6250	37.83230
$\mathbf{M_A}$ (g)	192	0.00	135,00	84.3750	37.83230
$\mathbf{C_T}$(days)	192	28.00	90.00	59.0000	31.08105
$\mathbf{C_{CO2}}$(%)	192	0.04	50.00	25.0200	25.04531
RH (%)	192	59.00	75.00	67.3333	3.86870
T (°C)	192	10.00	25.00	18.1667	4.44316
$\mathbf{E_T}$ (days)	192	7.00	360.00	113.1667	125.68644
$\mathbf{C_D}$ (mm)	192	0.00	14.80	5.3370	4.20344

Table 4

Data correlation coefficients

	C (g)	**M_A** (g)	**C_T**(days)	**C_{CO2}**(%)	**RH** (%)	**T** (°C)	**E_T**(days)	**C_D** (mm)
C (g)	1	-1.000**	0.000	0.000	0.000	0.000	0.000	-0.154*
M_A(g)	-1.000**	1	0.000	0.000	0.000	0.000	0.000	0.154*
C_T (days)	0.000	0.000	1	0.000	-0.086	0.038	0.000	-0.128
C_{CO2}(%)	0.000	0.000	0.000	1	-0.346**	0.414**	-0.772**	-0.388**
RH (%)	0.000	0.000	-0.086	-0.346**	1	-0.876**	0.355**	0.325**
T (°C)	0.000	0.000	0.038	0.414**	-0.876**	1	-0.167*	-0.051
E_T (days)	0.000	0.000	0.000	-0.772**	0.355**	-0.167*	1	0.757**
C_D (mm)	-0.154*	0.154*	-0.128	-0.388**	0.325**	-0.051	0.757**	1

* The correlation is significant at the 0.05 level (bilateral).
** The correlation is significant at the 0.01 level (bilateral).

Table 5

Estimation of R^2 versus the input data with different curves estimation regression models

Equations	***R^2***						
	C (g)	**M_A** (g)	**C_T**(days)	**C_{CO2}**(%)	**RH** (%)	**T** (°C)	**E_T**(days)
Linear	0.020	0.020	0.016	0.147	0.106	0.003	0.573
Quadratic	0.021	0.021	0.018	0.0151	0.131	0.078	0.6

2.5. ANN model development

The ANN are structures inspired by human brain and can be defined as a parallel and distributed system composed by processing units, called the neurons [52]. One of the merits of applying neural networks is that it can make models easy to use and more accurate from complex natural systems with large inputs [51, 72]. ANN contains an input layer, one or several hidden layers, and an output layer [1, 73]. The hidden and output layer are composed of computational neurons, each neuron receives weighted inputs from other neurons and communicates its outputs to other neurons by using an activation function. If the output of a node is greater than the specified threshold value, that node is activated and sends data to the next layer of the network. Otherwise, no data is transmitted to the next layer of the network.

The weighted sum of inputs components can be calculated as in Equation 1.

$$(\mathrm{net})_j = \sum_{i=1}^{n} W_{ij} * x_i b \tag{1}$$

Where $(\mathrm{net})_j$ is the weighted sum of the j neuron for the input received from the preceding layer, x_i is the output of the i neuron in the preceding layer and b is a fix value as internal addition.

For a particular problem, the number of neurons for the input layer and output layer is equal to the number of effective input variables and output variables respectively. All neurons in the input, hidden and output layers, are successively connected by weights and biases. For neural network the data is split into three subsets: training, validation and testing. The training of the network is done by Levenberg Marquardt algorithm. The most important part of training dataset is minimizing errors. This is achievable by changing the weights by a tan-sigmoid transfer function, during the learning step and continuing this until to find the optimal weight set. Once the network is trained, it can be used to validate against unseen data using trained weights and biases. This process is calling "validation". The validation dataset is used to assess the performance of model built in the training phase. Then, other tested data are used to determine the performance of the ANN model for predicting performance parameters. The network performance can be determined by calculating the mean square errors (MSE) Equation 2 and the determination coefficient (*R*)

Equation 3. For a better performance model, it should have a lower MSE (no error) and a higher *R* (best estimation).

$$\mathrm{MSE}\left(\sum_{i=1}^{N}(O_i - P_i)^2\right)/N \tag{2}$$

$$R = \frac{\sum_{i=1}^{N}(O_i - M_i)(P_i - N_i)}{\sqrt{\sum_{i=1}^{N}(O_i - M_i)^2 \sum_{i=1}^{N}(P_i - N_i)^2}} \tag{3}$$

Where O_i, P_i and M_i denote the observed or target values, ANN predicted values and the mean of O_i respectively. N represents the total number of data.

In this paper, 192 experimental measurements of carbonation depth were used in the ANN model (see Table 2). The network reported in this study is constructed and performed under the MATLAB program. The methodology presented in the typical structure of Fig. 1 was followed to determine a predictive model for the carbonation depth of mortars with different substitution levels of cement with MK, BP and CS. Initially, in order to provide the ANN model with good generalization capability, the database was randomly divided into three parts: (i) 70% for training (to train the network, through each pair of input/output), (ii) 15% for validation (to validate and to certify the trained network), and (iii) 15% for testing (to test and to check the model capabilities).

The architecture of the proposed model (ANN) contains seven input neurons, ten hidden neurons in the hidden layer, selected by trial and error, and one output neuron that is the carbonation depth (C_D), as illustrated in Fig. 1. The seven input datasets contained information about the mix proportions (M_A, C and C_T) and environmental conditions (C_{CO2}, RH, T, and E_T). The Levenberg–Marquardt (LM) algorithm was used to train the network, due to its suitable convergence, high precision, and reduced time consumption [51, 74-77]. The activation functions in the hidden and output layers were chosen as the hyperbolic tangent function Equation 4.

$$(\mathrm{Output})_j = \left(e^{\alpha(\mathrm{net})_j} - e^{-\alpha(\mathrm{net})_j}\right)/\left(e^{\alpha(\mathrm{net})_j} + e^{-\alpha(\mathrm{net})_j}\right) \tag{4}$$

Where: α is a constant used to control the slope of the semi-linear region and (Output) is carbonation depth (C_D). This function transforms the interval [–∞; +∞] to [–1; +1].

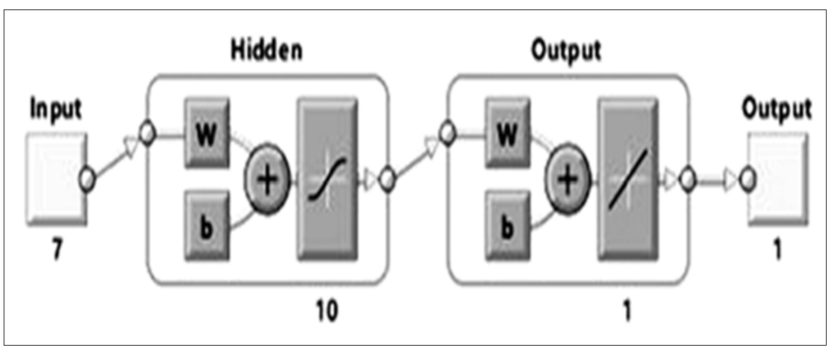

Fig. 1 - Neural network architecture

3. Results and discussion

3.1. Parametric analysis

3.1.1 Effect of SCMs content

The accelerated and natural carbonation depths are presented in Table 2. It appears that the natural carbonation results of mortars generally follow the same trend as those of accelerated carbonation.

The resistance to carbonation of mortars decreases with the increase of cement substitution by MK, BP or CS.

For the tow series of mortars: one after 28 days and another after 90 days curing ages, Fig. 2 shows the proportional relationship between the carbonation depths (C_D) measured on mortar specimens exposed to the accelerated carbonation during 7, 14 and 28 days, and the carbonation depths measured on mortar specimens exposed to the natural carbonation during 90, 180, and 360 days. A strong correlation was observed between the natural and accelerated carbonation, since the value of the linear regression coefficient is equal to 0.97.

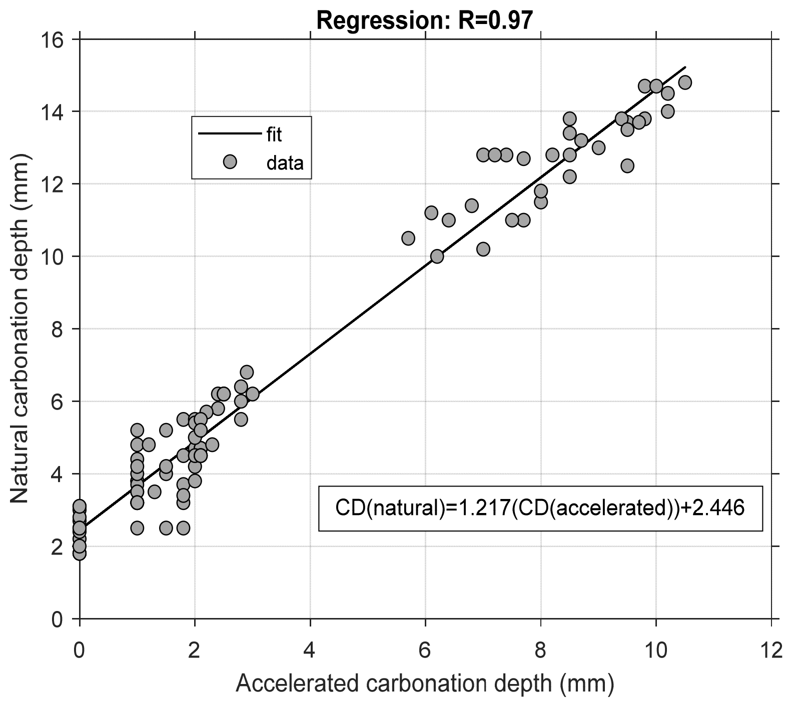

Fig. 2 - Correlation between accelerated and natural carbonation depths

Figs. 3, 4 and 5 show the effect of different admixture contents (0, 10, 15, 20, 25 and 30%) of MK, BP and CS, respectively on the natural and accelerated carbonation depth, considering the curing age (C_T) of 28 days. The results highlight that the carbonation depths in both conditions (natural and accelerated) of the mortars with MK, BP, or CS are generally higher than those of control mortar (CM). For instance, while the carbonation depth ranges from 0 to 11.2 for the control mortar, it reaches up to 14.8 (mm), 14.7 (mm) and 14 (mm) for mixes with 30% of MK, BP, and CS, respectively. This indicates between 25% and 32.1% more profound carbonation depths in mortars samples incorporating high amounts of MK, BP and CS as compared to that of the control mix (CM). In fact, the SCMs content can directly influence the carbonation rate of mortars, since this is highly dependent on the initial content of Portlandite that the cement material is more or less providing to the composition.

The control mortar (CM) presents very slow progress of carbonation (natural and accelerated), due to the initial content of Portlandite ($Ca(OH)_2$), and thereby greater resistance to carbonation than other mortars based on MK, BP and CS. According to Morandeau et al. [36], the consumption of Portlandite from cement hydration by the pozzolanic reactions of SCMs promotes the early carbonation of calcium silicate hydrate (CSH), leading to advanced carbonation depths as compared to the control mortar (CM). Fig. 6 shows the visual carbonation depths determined by phenolphthalein spraying of CM and mortars prepared with maximum contents of MK, BP, and

CS. The Fig. 6 shows the cross-sectional area of carbonated mortar specimens (40 × 40) mm^2, after 28 days of exposure to accelerated carbonation. These observations show that the ratio of the carbonated area of mortars with 30% of MK, BP, and CS are generally higher than those of CM, confirming that CM has greater carbonation resistance.

3.1.2 Effect of exposure time to CO_2

From Figs. 3, 4 and 5, the prime environmental factor influencing the carbonation rate of mortars is the exposure time to CO_2. A high depth increase can be observed when the exposure time to CO_2 increases. From 7 to 28 days of exposure to accelerated carbonation, an increase of 11.76%, 16.4%, 15% and 14.28% is recorded in the carbonation depth for CM, 30% MK, 30% BP and 30% CS-mortars, respectively. An increase of 26.7%, 35.37%, 34.28% and 28.37% is recorded in the carbonation depth for the same mortars from 90 to 360 days of exposure to natural carbonation.

When comparing the effect of each admixture, the use of MK resulted in the highest carbonation depths compared to BP and CS, respectively. This can be due to the greater pozzolanic reaction of MK and therefore a high consumption of CH, which causes higher carbonation of CSH products in this composition.

3.1.3 Effect of CO2 concentration

It can also be noticed from Figs. 3, 4 and 5, that the carbonation depths after 28 days of exposure to accelerated carbonation for different mortars used are more profound than carbonation depths after 90 and 180 days of exposure to natural carbonation. This may be attributed to a significantly higher CO_2 concentration in accelerated carbonation conditions, reaching approximately 50%, compared to the CO_2 concentration observed in natural carbonation, which is only around 0.04% [68].

The result shows that the natural carbonation depths of 360 days present the highest carbonation depths of all mortar mixes.

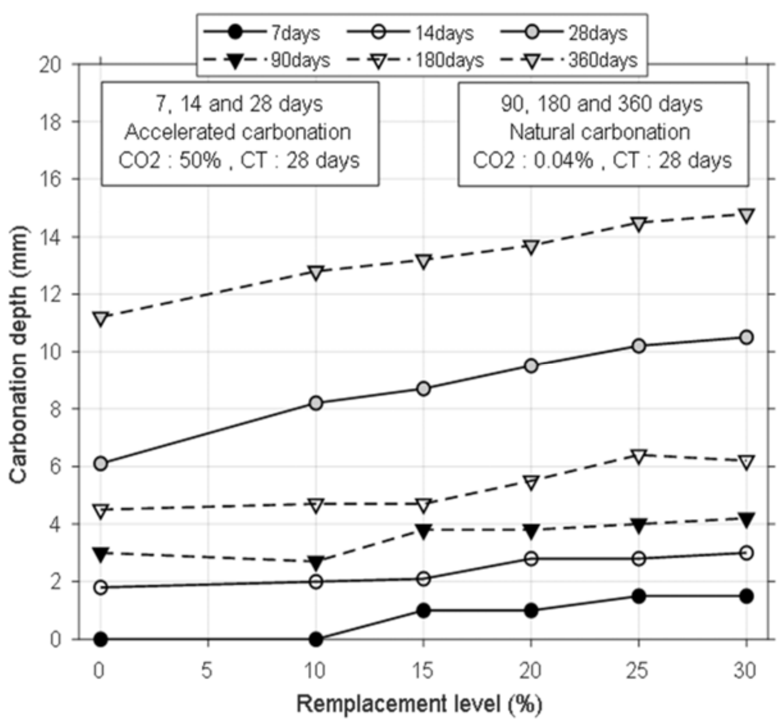

Fig. 3 - Effect of MK contents on mortar carbonation depth

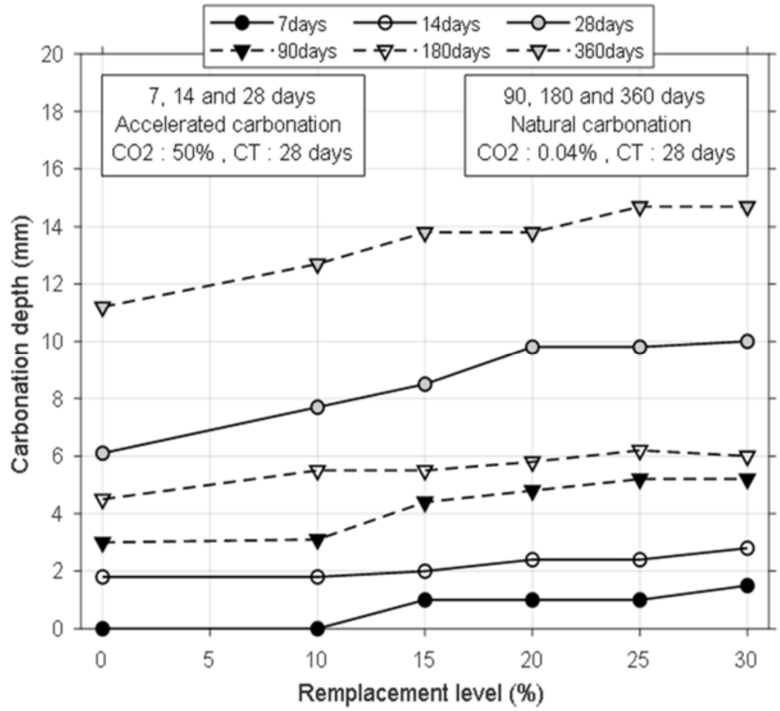

Fig. 4 - Effect of BP contents on mortar carbonation depth

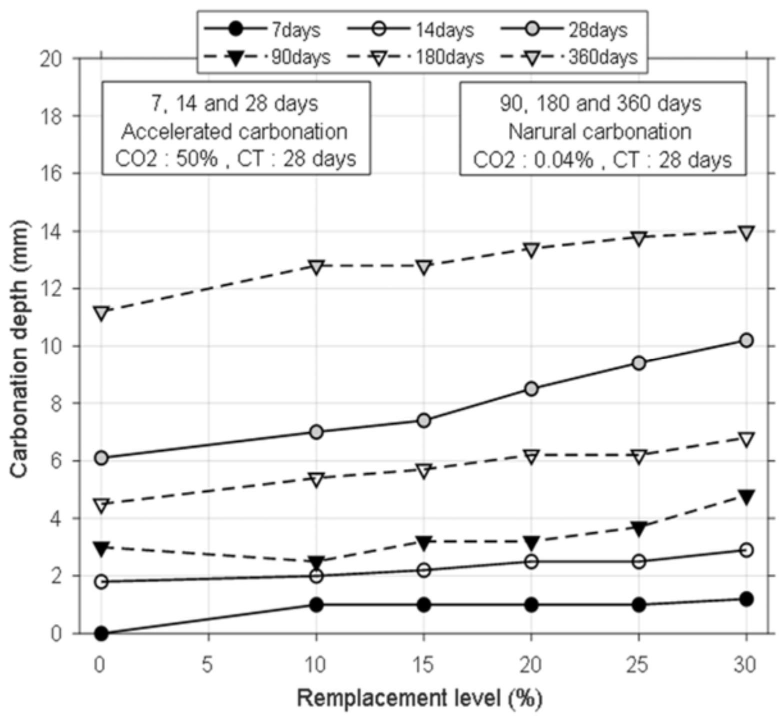

Fig. 5 - Effect of CS contents on mortar carbonation depth

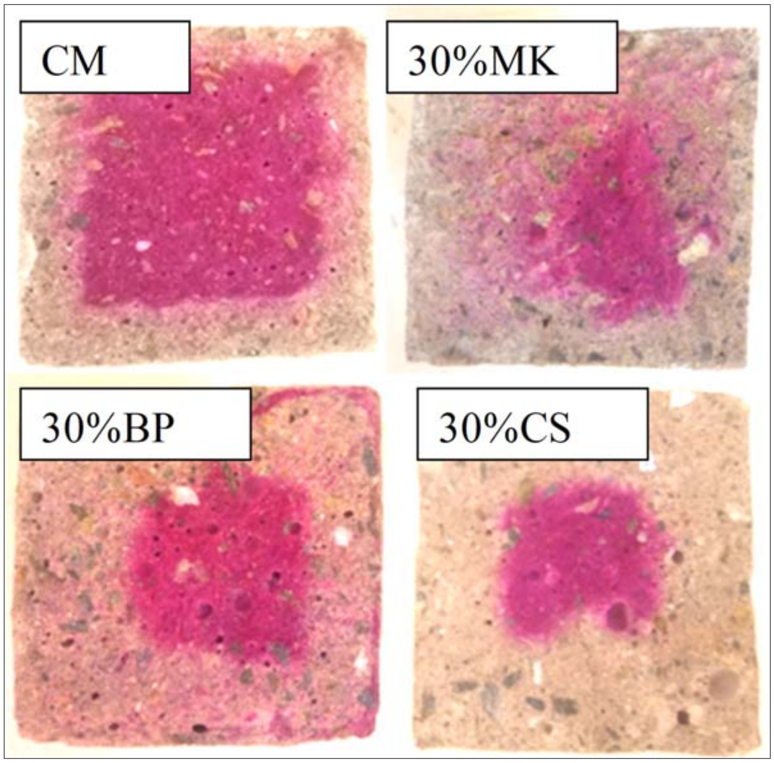

Fig. 6 - Visual depth of carbonated mortars exposed to 28 days of accelerated carbonation.

3.2. ANN modelling analysis

The obtained measurements of natural and accelerated carbonation depth of mortars containing MK, BP and CS can be predicted once the network is trained. Fig.7 represents the regression plot of the predicted versus experimental carbonation depth measurements for the training, validation and testing datasets. The correlation between the target (experimental data) and the ANN output as a function of the determination coefficient (*R*), for training, validation, testing and all data is provided in Fig. 7 (a), Fig. 7 (b), Fig.7 (c) and Fig.7 (d), respectively. Thus, by considering the seven input datasets contained information about the mix proportions (M_A, C and C_T) and environmental conditions (C_{CO2}, RH, T, and E_T), the predicted carbonation depth model is described in the following Equations 5 to 9:

$$\mathrm{Output} = \mathrm{b_2} + \mathrm{LW} \cdot \tanh(\mathrm{b_1} + \mathrm{IW} \cdot \mathrm{X}) \tag{5}$$

Where: X is input value.

$$\mathrm{b_1} = \begin{pmatrix} 1.9231 \\ 1.3851 \\ -1.3748 \\ -0.6456 \\ 0.3266 \\ -0.9835 \\ 0.6766 \\ -0.8097 \\ 2.1589 \\ 2.1402 \end{pmatrix} \tag{6}$$

$$\mathrm{b_2} = (0.2843) \tag{7}$$

$$\mathrm{IW}=\begin{pmatrix} -1.2938 & -0.1804 & -0.8967 & 0.5488 & 0.5359 & 0.6628 & -0.7724 \\ -1.2672 & -0.3052 & -0.4325 & 0.8353 & 1.0967 & -1.1958 & 0.0032 \\ 0.9253 & 0.7671 & 0.4840 & -0.3854 & -0.2355 & -0.0033 & 1.0804 \\ 0.9501 & 0.6971 & -0.8177 & 0.1910 & 0.9164 & -0.3744 & -0.8427 \\ -0.9267 & 0.5775 & -0.5720 & -0.7410 & -0.8212 & -0.3324 & 0.8948 \\ -0.1347 & -0.2255 & -0.0188 & -0.0589 & -1.6110 & -1.1081 & -1.2732 \\ 0.2268 & 1.2929 & -0.6574 & 0.8500 & -0.3585 & 0.1099 & 0.8212 \\ -0.7348 & -0.5864 & -0.0315 & 2.9250 & -0.6549 & -0.5308 & 2.9954 \\ 0.6674 & 0.1626 & 0.0805 & -0.2736 & -0.3197 & -0.9404 & 1.1867 \\ 0.3457 & 0.8677 & -0.1809 & -0.5284 & -0.5017 & -1.0338 & -0.8867 \end{pmatrix} \tag{8}$$

$$\mathrm{LW}=\begin{pmatrix} -01985 & -0.2028 & -0.7029 & 0.0341 & 0.1130 & -1.5147 & 0.0786 & 3.1110 & 0.8835 & 0.5827 \end{pmatrix} \tag{9}$$

Furthermore, the determination coefficient (R) and the mean squared error (MSE) of the network performance found from training, validation and testing are given in Table 6. From this table, the determination coefficients found are 99.3% for the training, 98.8% for the validation and 99.2% for the testing dataset. As can be seen, the statistical values of the mean square error (MSE) from training, validation and testing sets in ANN model are 0.214, 0.301 and 0.350, respectively. It is clearly noticed that the model gives a lower mean squared error (MSE) with a higher determination coefficient (R), which indicates a perfect correlation between the experimental measurements and the predicted carbonation depth of different mixes of mortar used. This further confirms the suitability of the proposed ANN model.

The errors percentage rates of carbonation depth reached from training, validation and testing in ANN model are given in Fig. 8. The errors between the target and output values range between -0.952 and 1.294 for all the input values. From the results presented above, the developed model shows superior performance in predicting the carbonation depth of MK, BP and CS modified mortar, which is consistent with what is expected from traditional approaches.

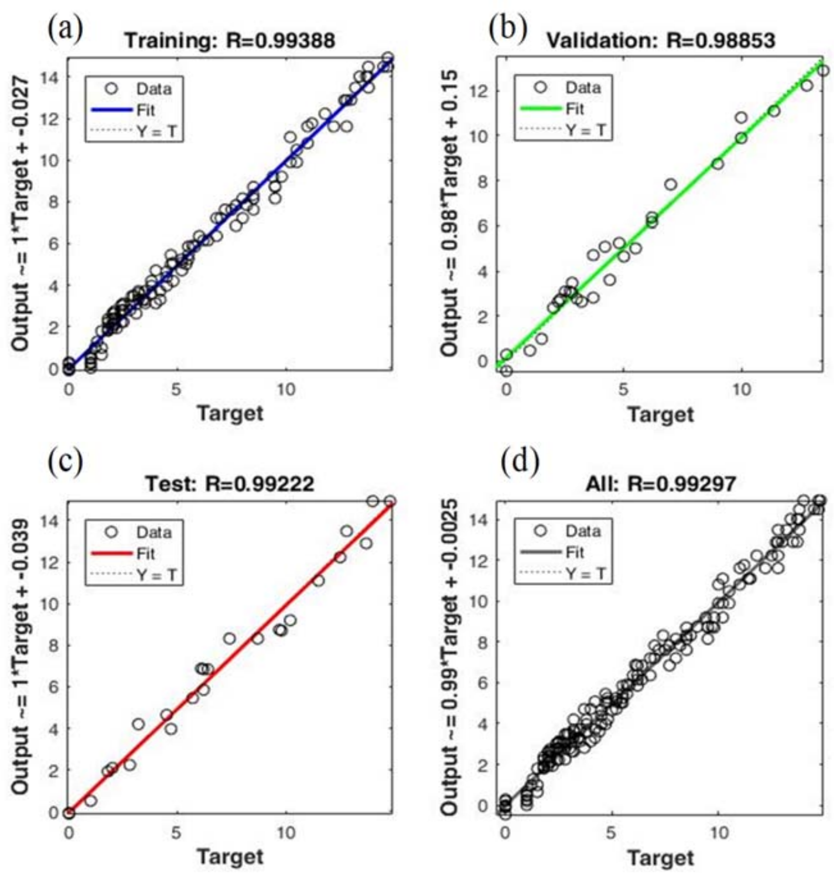

Fig. 7 - Training data, validation, testing and all results of ANN

Table 6

Performance results of the developed ANN model

	Carbonation depth		
	Training set	**Validation**	**Testing set**
Samples	134	29	29
MSE	0.214	0.301	0.350
R	0.993	0.988	0.992

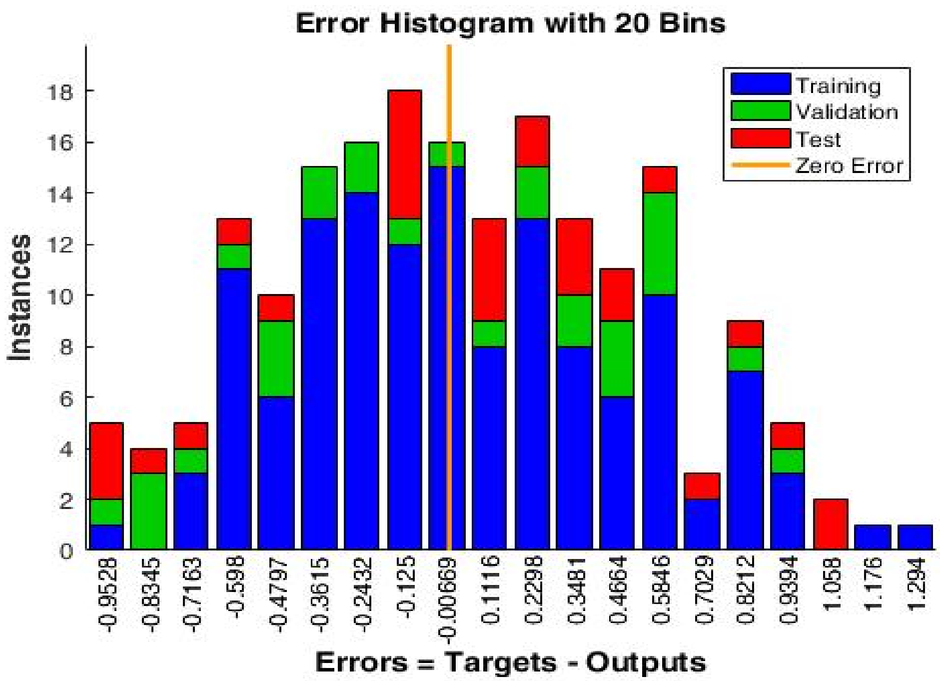

Fig. 8 - Errors results between targets and outputs of carbonation depth

4. Conclusion

This paper investigated the reliability of the artificial neural network approach to predict the carbonation depth of metakaolin, brick powder and calcined sediments-modified mortars. The ANN modelling was based on the main influential factors on mortar carbonation, including the SCMs content (M_A), cement content (C), curing time (C_T), CO_2 concentration (C_{CO2}), relative humidity (RH), temperature (T) and CO_2 exposure time (E_T). An experimental data-set with 192 measurements of natural and accelerated carbonation depth was used. Based on observed results, the following conclusions can be drawn:

Modified mortars with MK, BP and CS as SCMs, decrease the carbonation resistance as the cement substitution rate by MK, BP and CS increases.

Carbonation depth of different mortars tested is influenced much more by the MK, BP and CS content, cement content, CO_2 concentration and exposure time to CO_2.

Correlation analysis between the natural and accelerated carbonation depth (C_D) can be approximated by a linear fit with a high regression coefficient.

The ANN developed with seven input neurons, ten hidden neurons in the hidden layer and one output neuron (carbonation depth (C_D)), shows the best integral performance with the lower mean squared error (MSE) and the higher determination coefficient (*R*), which indicates that the carbonation depth of MK, BP and CS-based mortars can accurately be predicted by using the ANN model developed.

The carbonation depth of mortars with low clinker content can correctly be predicted by ANN model, without attempting any experiments, which can be useful to save the required energy, time and cost.

Experimental measurements of the natural and accelerated carbonation depth of MK, BP and CS-modified mortars tested are therefore of importance in order to enrich the literature and improve the reliability and the robustness of the proposed ANN model for predicting carbonation depth.

Acknowledgments

The authors would thank the Civil Engineering Laboratory and the Smart Structures Laboratory (SSL), of Aïn-Temouchent University for providing the necessary equipment to perform the experimental work of this research.

References

[1] Liu K., Alam M.S., Zhu J., Zheng J. & Chi L. (2021). Prediction of carbonation depth for recycled aggregate concrete using ANN hybridized with swarm intelligence algorithms. *Constr. Build. Mater.* 301, 124382. DOI: 10.1016/j.conbuildmat.2021.124382.

[2] Schneider M. (2019). The cement industry on the way to a low-carbon future. *Cem. Concr. Res.* 124, 105792. DOI: 10.1016/j.cemconres.2019.105792.

[3] Robbie-Andrew M. (2018). Global CO_2 emissions from cement production. *J. Earth. Syst. Sci. Data*. 10, 195-217. DOI: 10.5194/essd-10-195-2018.

[4] Benhelal E., Shamsaei E. & Rashid M.I. (2021). Challenges against CO_2 abatement strategies in cement industry: A review. *J. Environ. Sci.* 104, 84-101. DOI: 10.1016/j.jes.2020.11.020.

[5] Chatterjee A. & Sui T. (2019). Alternative fuels–effects on clinker process and properties. *Cem. Concr. Res.* 123, 105777. DOI: 10.1016/j.cemconres.2019.105777.

[6] Yang D.Y., Liu M. & Ma Z.M. (2020). Properties of the foam concrete containing waste brick powder derived from construction and demolition waste. *J. Build. Eng.* 32, 101509. DOI: 10.1016/j.jobe.2020.101509.

[7] Zhao Y., Gao J., Liu C., Chen X. & Xu Z. (2020). The particle-size effect of waste clay brick powder on its pozzolanic activity and properties of blended cement. *J. Clean. Prod*. 242, 118521. DOI: 10.1016/j.jclepro.2019.118521.

[8] Güneyisi E. & Mermerdaş K. (2007). Comparative study on strength, sorptivity, and chloride ingress characteristics of air-cured and water-cured concretes modified with metakaolin. *Mater. Struct*. 40, 1161-1171. DOI: 10.1617/s11527-007-9258-5.

[9] Komnitsas K., Zaharaki D., Vlachou A., Bartzas G. & Galetakis M. (2015). Effect of synthesis parameters on the quality of construction and demolition wastes (CDW) geopolymers. *Adv. Powder. Technol*. 26, 368–376. DOI: 10.1016/j.apt.2014.11.012.

[10] Parande A.K., Babu B.R., Karthik M.A., Kumaar K.D. & alaniswamy N. (2008). Study on strength and corrosion performance for steel embedded in metakaolin blended concrete/mortar. *Constr. Build. Mater.* 22, 127–134. DOI: 10.1016/j.conbuildmat.2006.10.003.

[11] Said-Mansour M., Kadri E.H., Kenai S., Ghrici M. & Bennaceur R. (2011). Influence of calcined kaolin on mortarproperties. *Constr. Build. Mater*. 25, 2275-2282. DOI: 10.1016/j.conbuildmat.2010.11.017.

[12] Ouldkhaoua Y., Benabed B., Abousnina R., Kadri E.H. & Khatib J. (2020). Effect of using metakaolin as supplementary cementitious material and recycled CRT funnel glass as fine aggregate on the durability of green self-compacting concrete. *Constr. Build. Mater.* 235, 117802. DOI: 10.1016/j.conbuildmat.2019.117802.

[13] Khatib J.M. & Clay R.M. (2004). Absorption characteristics of metakaolin concrete. *Cem. Concr. Res.* 34, 19-29. DOI: 10.1016/S0008-8846(03)00188-1.

[14] Vejmelková E., Keppert M., Grzeszczyk S., Skaliński B. & Černý R. (2011). Properties of self-compacting concrete mixtures containing metakaolin and blast furnace slag. *Constr. Build. Mater.* 25, 1325-1331. DOI: 10.1016/j.conbuildmat.2010.09.012.

[15] Bernal S.A., De Gutiérrez R.M. & Provis J.L. (2012). Engineering and durability properties of concretes based on alkali-activated granulated blast furnace slag/metakaolin blends. *Constr. Build. Mater*. 33, 99-108. DOI: 10.1016/j.conbuildmat.2012.01.017.

[16] Badogiannis E. & Tsivilis S. (2009). Exploitation of poor Greek kaolins: Durability of metakaolin concrete. *Cem. Concr. Compos*. 31, 128-133. DOI: 10.1016/j.cemconcomp.2008.11.001.

[17] Barbhuiya S., Chow P. & Memon S. (2015). Microstructure, hydration and nanomechanical properties of concrete containing metakaolin. *Constr. Build. Mater.* 95, 696-702. DOI: 10.1016/j.conbuildmat.2015.07.101.

[18] Schackow A., Stringari D., Senff L., Correia S.L. & Segadães A.M. (2015). Influence of fired clay brick waste additions on the durability of mortars. *Cem. Concr. Compos.* 62, 82–89. DOI: 10.1016/j.cemconcomp.2015.04.019.

[19] Silpa K., Lisa Y., Perinaz B.T. & Frank V.W. (2018). What a waste 2.0: a global snapshot of solid waste management to 2050, World Bank Publications. *https://openknowledge.worldbank.org/handle/10986/30317.*

[20] Pasupathy K., Ramakrishnan S. & Sanjayan J. (2021). Formulating eco-friendly geopolymer foam concrete by alkali-activation of ground brick waste. *J. Clean. Prod.* 325, 129180. DOI: 10.1016/j.jclepro.2021.129180.

[21] Ma Z.M., Liu M., Tang Q., Liang C.F. & Duan Z. (2019). Chloride permeability of recycled aggregate concrete under the coupling effect of freezing-thawing, elevated temperature or mechanical damage. *Constr. Build. Mater*. 237, 117648. DOI: 10.1016/j.conbuildmat.2019.117648.

[22] Grellier A., Bulteel D., Bouarroudj M.E.K., Rémond S., Zhao Z. & Courard L. (2021). Alternative hydraulic binder development based on brick fines: Influence of particle size and substitution rate. *J. Build. Eng.* 39, 102263. DOI: 10.1016/j.jobe.2021.102263.

[23] Safhi A.M., Rivard P., Yahia A., Benzerzour M. & Khayat K.H. (2021). Valorization of dredged sediments in self-consolidating concrete: fresh, hardened, and microstructural properties. *J. Clean. Prod*. 263, 121472. DOI: 10.1016/j.jclepro.2020.121472.

[24] Sadok R.H., Belas N., Tahlaiti M. & Mazouzi R. (2021). Reusing calcined sediments from Chorfa II dam as partial replacement of cement for sustainable mortar production. *J. Build. Eng*. 40, 102273. DOI: 10.1016/j.jobe.2021.102273.

[25] Jaglal K., Crawford D.M., Anagnost S.W. & White B.E. (2017). Alternative Approaches for Managing Dredged Sediments, in: Proceeding of the Western Dredging Association (WEDA), Vancouver, British Columbia, Canada.

[26] Ortega J.M., Letelier V., Solas C., Moriconi G., Climent M.A. & Sánchez I. (2018). Longterm effects of waste brick powder addition in the microstructure and service properties of mortars. *Constr. Build. Mater.* 182, 691–702. DOI: 10.1016/j.conbuildmat.2018.06.161.

[27] Li L.G., Lin Z.H., Chen G.M. & Kwan A.K.H. (2020). Reutilizing clay brick dust as paste substitution to produce environment-friendly durable mortar. *J. Clean. Prod*. 274, 122787. DOI: 10.1016/j.jclepro.2020.122787.

[28] Kazi Aoual-Benslafa F., Kerdal D., Ameur M., Mekerta B. & Semcha A. (2015). Durability of mortars made with dredged sediments. *Proc. Eng.* 118, 240–25. DOI: 10.1016/j.proeng.2015.08.423.

[29] Safer O., Belas N., Belaribi O., Belguesmia K., Bouhamou N.E. & Mebrouki A. (2018). Valorization of dredged sediments as a component of vibrated concrete: durability of these concretes against sulfuric acid attack. *Int. J. Concr. Struct. Mater*. 12, 44. DOI: 10.1186/s40069-018-0270-7.

[30] Belguesmia K. (2018). Optimization of an Eco-BAP Based on Dredged Sediment of Fresh, Hardened and Durability, Thesis. Abdelhamid Ibn Badis University of Mostaganem.

[31] Taffese W.Z. &Sistonen E. (2013). Service life prediction of repaired structures using concrete recasting method: state-of-the-art. *Proc. Eng.* 57, 1138–114. DOI: 10.1016/j.proeng.2013.04.143.

[32] Kari O.P., Puttonen J. & Skantz E. (2014). Reactive transport modelling of long-term carbonation. *Cem. Concr. Compos*. 52, 42–53. DOI: 10.1016/j.cemconcomp.2014.05.003.

[33] Taffese W.Z., Sistonen E. & Puttonen J. (2015). CaPrM: Carbonation prediction model for reinforced concrete using machine learning methods. *Constr. Build. Mater*. 100, 70-82. DOI: 10.1016/j.conbuildmat.2015.09.058.

[34] Yang K.H., Singh J., Lee B.Y. & Kwon S.J. (2017). Simple technique for tracking chloride penetration in concrete based on the crack shape and width under steady-state conditions. *Sustainability.* 9, 282.

[35] Papadakis V.G. (2000). Effect of supplementary cementing materials on concrete resistance against carbonation and chloride ingress. *Cem. Concr. Res.* 30, 291-299. DOI: 10.1016/S0008-8846(99)00249-5.

[36] Morandeau A., Thiery M. & Dangla P. (2014). Investigation of the carbonation mechanism of CH and CSH in terms of kinetics, microstructure changes and moisture properties. *Cem. Concr. Res*. 56, 153-170. DOI: 10.1016/j.cemconres.2013.11.015.

[37] Duan P., Shui Z., Chen W. & Shen C. (2015). Enhancing microstructure and durability of concrete from ground granulated blast furnace slag and metakaolin as cement replacement materials. *J. Mater. Res. Techno.* 2, 52-59. DOI: 10.1016/j.jmrt.2013.03.010.

[38] Bernal S.A. (2015). Effect of the activator dose on the compressive strength and accelerated carbonation resistance of alkali silicate-activated slag/metakaolin blended materials. *Constr. Build. Mater*. 98, 217-226. DOI: 10.1016/j.conbuildmat.2015.08.013.

[39] Singh N., Mithulraj M. & Arya S. (2019). Utilization of coal bottom ash in recycled concrete aggregates based self compacting concrete blended with metakaolin, Resources. *Conser. Recycl.* 144, 240-251. DOI: 10.1016/j.resconrec.2019.01.044.

[40] Güneyisi E., Gesoğlu M. & Mermerdaş K. (2008). Improving strength, drying shrinkage, and pore structure of concrete using metakaolin. *Mater. Struct.* 41, 937-949. DOI: 10.1617/s11527-007-9296-z.

[41] Ramezanianpour A.A. & Jovein H.B. (2012). Influence of metakaolin as supplementary cementing material on strength and durability of concretes. *Constr. Build. Mater.* 30, 470-479. DOI: 10.1016/j.conbuildmat.2011.12.050.

[42] Poon C.S., Kou S.C. & Lam L. (2006). Compressive strength, chloride diffusivity and pore structure of high performance metakaolin and silica fume concrete. *Constr. Build. Mater.* 20, 858-865. DOI: 10.1016/j.conbuildmat.2005.07.001.
[43] Safer O. (2017). Optimization of the formulation of an eco-concrete based on dredging sediments and study of its resistance to chemical attacks. PhD Dissertation. Mostaganem University, Algeria.
[44] Mikhailenko P., Cassagnabère F., Emam A. & Lachemi M. (2018). Influence of physico-chemical characteristics on the carbonation of cement paste at high replacement rates of metakaolin. *Constr. Build. Mater.* 158, 164-172. DOI: 10.1016/j.conbuildmat.2017.10.021.
[45] Shao J.H. (2019). Hydration performance and carbonation of clay brick powder-cement complex cementitious material. Doctoral dissertation, Master thesis, Southeast University. China.
[46] Ekolu S.O. (2018). Model for practical prediction of natural carbonation in reinforced concrete: Part 1-formulation. *Cem. Concr. Compos*. 86, 40–56. DOI: 10.1016/j.cemconcomp.2017.10.006.
[47] Félix E.F., Carrazedo R. & Possan E. (2017). Parametric analysis of carbonation process in reinforced concrete structures through Artificial Neural Networks. *Revista. ALCONPAT.* 7, 302–316. DOI: 10.21041/ra.v7i3.245.
[48] Van Balen K. & Van Gemert D. (1994). Modelling lime mortar carbonation. *Mater. Struct.* 27, 393-398.
[49] Papadakis V.G., Vayenas C.G. & Fardis M.N. (1991). Fundamental modelling and experimental investigation of concrete carbonation. *Mater. J.* 88, 363-373.
[50] Haykin S. (2007). Neural Networks: A Comprehensive Foundation, Prentice-Hall Inc.
[51] Moradi M.J., Khaleghi M., Salimi J., Farhangi V. & Ramezanianpour A.M. (2021). Predicting the compressive strength of concrete containing metakaolin with different properties using ANN. *Meas*.183, 109790. DOI: 10.1016/j.measurement.2021.109790.
[52] Felix E.F., Carrazedo R. & Possan E. (2021). Carbonation model for fly ash concrete based on artificial neural network: Development and parametric analysis. *Constr. Build. Mater.* 266, 121050. DOI: 10.1016/j.conbuildmat.2020.121050.
[53] Akpinar P. & Uwanuakwa F.I.D. (2016). Intelligent prediction of concrete carbonation depth using neural networks, Bull. Transilvania Univ. Brasov. *Math. Informat. Phys.* Series III.9, 99.
[54] Lu C. & Liu R. (2009). Predicting carbonation depth of prestressed concrete under different stress states using artificial neural network. *Adv. Artificial. Neural. Syst*. DOI: 10.1155/2009/193139.
[55] Kwon S.J. & Song H.W. (2010). Analysis of carbonation behavior in concrete using neural network algorithm and carbonation modelling. *Cem. Concr. Res.* 40, 119–127. DOI: 10.1016/j.cemconres.2009.08.022.
[56] Han-Seung L. & Wang X.Y. (2016). Evaluation of compressive strength development and carbonation depth of high volume slag-blended concrete. *Constr. Build. Mater*. 124, 45–54. DOI: 10.1016/j.conbuildmat.2016.07.070.
[57] Londhe S.N., Kulkarni P.S., Dixit P.R., Silva A., Neves R. & Brito J. (2021). Predicting carbonation coefficient using Artificial neural networks and genetic programming. *J. Build. Eng*. 39, 102258. DOI: 10.1016/j.jobe.2021.102258.
[58] Possan E., Thomaz W.A., Aleandri G.A., Felix E.F. & dos Santos A.C. (2017). CO_2 uptake potential due to concrete carbonation: a case study. *Case. Stud. Constr. Mater*. 6, 147–161. DOI: 10.1016/j.cscm.2017.01.007.
[59] Luo D., Niu D. & Dong Z. (2014). Application of neural network for concrete carbonation depth prediction. *4th International Conference on the Durability of Concrete Structures.*
[60] Carevic V., Ignjatovic I. & Dragaš J. (2019). Model for practical carbonation depth prediction for high volume fly ash concrete and recycled aggregate concrete. *Constr. Build. Mater.* 213, 194–208. DOI: 10.1016/j.conbuildmat. 2019.03.267.
[61] Kellouche Y., Boukhatem B., Ghrici M. & Tagnit-Hamou A. (2019). Exploring the major factors affecting fly-ash concrete carbonation using artificial neural network. *Neural. Comput. Appl*. 31, 969–988. DOI: 10.1007/s00521- 017-3052-2.
[62] Jiang L., Lin B. & Cai Y. (2000). A model for predicting carbonation of high-volume fly ash concrete. *Cem. Concr. Res.* 30, 699-702. DOI: 10.1016/S0008-8846(00)00227-1.
[63] Chérifi W.N.E.H., Houmadi Y. & Aissa Mamoune S.M. (2022). Prediction of corrosion potential using the generalized artificial neural networks method. *Can. J. Civ. Eng.* 49(6), 1040-1048. DOI: 10.1139/cjce-2020-0712.
[64] Limeira J., Etxeberria M., Agullo L. & Molina D. (2011). Mechanical and durability properties of concrete made with dredged marine sand, *Constr. Build. Mater.* 25(11), 4165–4174. DOI: 10.1016/j.conbuildmat.2019.117178.
[65] EN 197-1 (2011). Standard Cement – Part 1- Composition, specifications and conformity criteria for common cements.
[66] Afnor, NF EN 196-1 (2016). Methods of Testing Cement - Part 1: Determination of Strength.
[67] AFGC–AFREM (1997). Recommended Method for Durability Indicator, Proceedings of the Technical Meeting of AFPC–AFREM, Toulouse, France.
[68] Auroy M., Poyet S., Le Bescop P., Torrenti J.M., Charpentier T., Moskura M. & Bourbon X. (2018). Comparison between natural and accelerated carbonation (3% CO_2): Impact on mineralogy, microstructure, water retention and cracking, *Cem. Concr. Res.* 109, 64-80. DOI: 10.1016/j.cemconres.2018.04.012.

[69] Benjamin J.R. & Cornell C.A. (1970). Probability, Statistics and Decision for Civil Engineers, Mcgraw-Hill Book Company, New York, USA. 684. ISBN 07004549-6.

[70] Subir P. (2012). Modelling to Study the Effect of Environmental Parameters on Corrosion of Mild Steel in Seawater Using Neural Network. *Int. Sch. Res. Netw.* ISRN Metallurgy: 6. DOI: 10.5402/2012/487351.

[71] Haykin S. (2009). Neural networks and learning machines, 3rdedn. Pearson Education Inc, Upper Saddle River.

[72] Abiodun O.I., Jantan A., Omolara A.E., Dada K.V., Mohamed N.A. & Arshad H. (2018). State-of-the-art in artificial neural network applications: A survey. *Heliyon.* 4, e00938. DOI: 10.1016/j.heliyon.2018.e00938.

[73] Adhikary B.B. & Mutsuyoshi H. (2006) Prediction of shear strength of steel fiber RC beams using neural networks. *Constr. Build. Mater*. 20, 801–811. DOI: 10.1016/j.conbuildmat.2005.01.047.

[74] Hosseinpour M., Sharifi H. & Sharifi Y. (2018). Stepwise regression modelling for compressive strength assessment of mortar containing metakaolin. *Int. J. Model. Simul.* 38, 207–215. DOI: 10.1080/02286203.2017.1422096.

[75] McCulloch W. & Pitts W. (1943). A logical calculus of the ideas immanent in nervous activity. *Bull. Math. Biophys.* 5, 115–133. DOI: 10.1007/BF02478259.

[76] Rahali B., Aissa Mamoune S.M. & Trouzine H. (2018). Using artificial neural networks approach to estimate compressive strength for rubberized concrete. *Period. Polytech. Civ. Eng.* 62, 858-865. DOI: 10.3311/PPci.11928.

[77] Merouane F.Z. & Aissa Mamoune S.M. (2019). Prediction of Swelling Parameters of Two Clayey Soils from Algeria using Artificial Neural Networks. *Mathe. Model. Civ. Eng.* 14(3), 11-26. DOI: 10.2478/mmce-2018-0008.